Fabrication of Large-area Micro-lens Arrays with Fast Tool Control

Young Jin Noh[1,#], Yoshikazu Arai[1], Makoto Tano[1] and Wei Gao[1]

1 Nano-metrology and Control Laboratory, Department of Nanomechanics, Tohoku University, Aramaki Aza Aoba 6-6-01, Sendai, 980-8579, Japan
Corresponding Author / E-mail: yjnoh@nano.mech.tohoku.ac.jp, TEL: +81-22-795-6953, FAX: +81-22-795-6953

KEYWORDS: Fast tool control, Force sensor, Micro-lens arrays

This paper describes a fast tool control (FTC)-based diamond turning process for fabricating large-area high-quality micro-lens arrays. The developed FTC unit has a stroke of 48 μm and a resonance frequency of 4.9 kHz. Micro-lens arrays were fabricated using a micro-cutting tool with a nose radius of 50 μm. The FTC unit was integrated with a force sensor so that the initial position of the micro-cutting tool with respect to the workpiece surface could be detected through monitoring the contacting force. The length and depth of the designed parabolic micro-lens profile were 190 μm and 20 μm, respectively. A micro-lens array was fabricated on a cylinder surface over an area of ϕ 55 mm × 40 mm.

Manuscript received: February 4, 2008 / Accepted: July 3, 2008

1. Introduction

Micro-lens arrays are expected to be used in flat panel displays (FPDs), including liquid crystal displays (LCDs), to improve the brightness distribution and expand the view angles.[1] The size of manufactured FPDs has been increasing, requiring the fabrication of high-quality large-area micro-lens arrays. Optical and electronic fabrication methods for such 3D microstructures include photolithography, electron beam writing, and focused ion beam machining.[2-4] Although these methods are effective for fabricating microstructures with pitches of sub-micrometer order, they require a long period of time to fabricate microstructures over large areas. It is also difficult for these methods to generate three-dimensional profiles of microstructures accurately, something that is essential for the micro-lens arrays used in FPD applications.[5]

Mechanical cutting is a traditional precision fabrication method that has been well adapted to fabricate large-area surfaces with a high degree of accuracy.[6,7] It is also possible for single-point diamond cutting to generate middle-pitched microstructures over large areas, provided there is fast control of the diamond cutting tool.[8-10] The pitches of the micro-lens arrays for FPD applications range from tens of micrometers to hundreds of micrometers, a length scale that is within the capability of single-point diamond cutting. The accuracy of the form and surface finish of the machined surface can be ensured with accurate motion of the diamond turning machine and a sharp single-crystal diamond cutting tool edge. For these reasons, single-point diamond cutting together with fast tool control shows the most potential as a suitable fabrication method for micro-lens arrays.

When fabricating micro-lenses, their geometry makes it necessary to use a micro-diamond cutting tool with a very small nose radius and a large clearance angle. Since the tool tip is very fragile, if the contact between the micro-cutting tool and the workpiece cannot be precisely controlled, the tool can be easily damaged. Therefore, the challenge is to detect contact between the tool and workpiece so as to determine the initial machining position. The contact process is conventionally monitored by using optical microscopes or the naked eye, but these methods are unable to observe the chips and cutting marks generated by micro-cutting. To make contact detection easier, it is desirable to automate the detection process.

This paper describes a fast tool control (FTC) unit integrated with a force sensor that can automatically detect the contact between the workpiece surface and the micro-cutting tool. After a description of the design and construction of the FTC unit, the results obtained when fabricating a large-area micro-lens array are presented.

2. The FTC unit

A schematic diagram of the fabrication system on a diamond turning machine is shown in Figure 1. A cylindrical workpiece is mounted on the spindle with its rotation about the X axis. The X slide is used to move the FTC unit along the X axis. Combining the in-feed motion from the FTC unit, the cross-feed motion from the X slide and the cutting motion from the spindle enables fabrication over a large area. The pitches of the micro-lens array along the circumference and axial directions of the cylindrical workpiece are assumed to be P_C and P_A, respectively.

Figure 2 shows a single-point diamond tool, a hollow PZT actuator, a capacitance displacement sensor, and a piezoelectric force sensor, all located within the FTC unit. The PZT actuator is used to generate the in-feed motion of the tool. The displacement of the PZT actuator is measured by the displacement sensor that is mounted inside the hollow of the PZT actuator. The force sensor is attached to the front end of the PZT actuator to improve its sensitivity.[11]

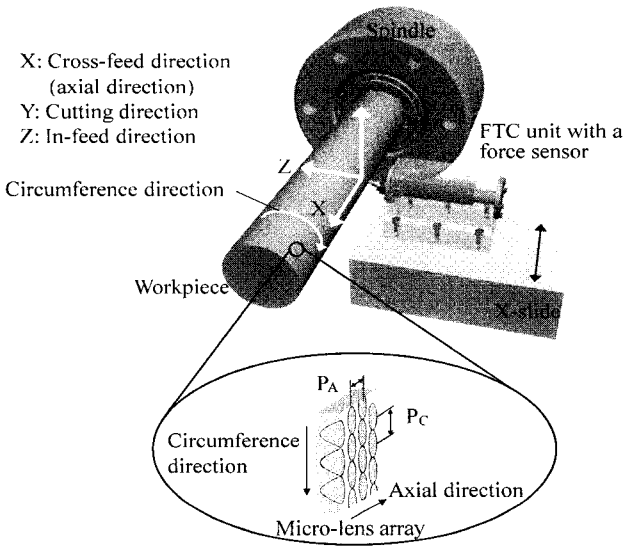

Fig. 1 Schematic diagram of the fabrication system with an FTC unit

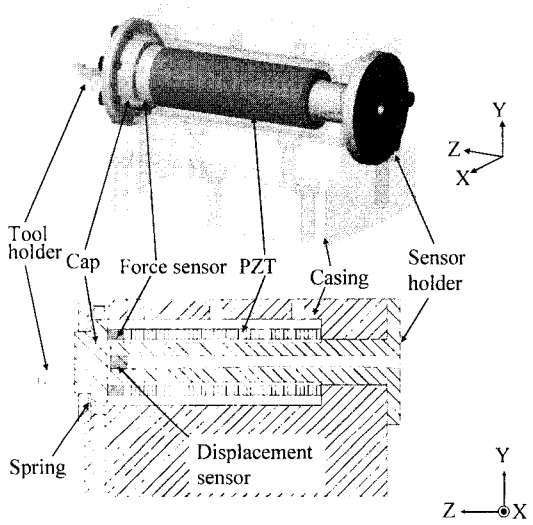

Fig. 2 Structure of the FTC unit integrated with a force sensor

Because the PZT actuator can only produce high pushing forces and cannot withstand large tensile forces, a wave washer is employed as a spring to apply a preload to the PZT actuator and obtain a balanced push and pull performance. The length, inner diameter, and outer diameter of the PZT actuator are 60 mm, 14 mm, and 20 mm, respectively. The force sensor, which also has a hollow shape, is 5 mm in length. The inner and outer diameters are the same as those of the PZT actuator. The displacement sensor has a measurement range of 125 μm, larger than the 48-μm stroke of the PZT actuator. The displacement sensor has dimensions of ϕ 3.9 × 9.5 mm, which makes it small enough to mount inside the PZT actuator. The displacement sensor has a maximum bandwidth of 20 kHz.

The stiffness and frequency response are the most important characteristics of a FTC unit. The stiffness of the entire unit is essentially determined by the stiffness of each element within it. The model shown in Figure 3 was developed to analyze the stiffness. The moving elements include the head (tool holder and tool cap), force sensor, and PZT actuator. Each moving element is assumed to be elastic. Hence, the stiffness of the entire FTC unit in the Z direction can be expressed by:

$$K_Z = \frac{1}{\frac{1}{k_h}+\frac{1}{k_f}+\frac{1}{k_p}} = \frac{k_h k_f k_p}{k_f k_p + k_h k_p + k_h k_f} \quad (1)$$

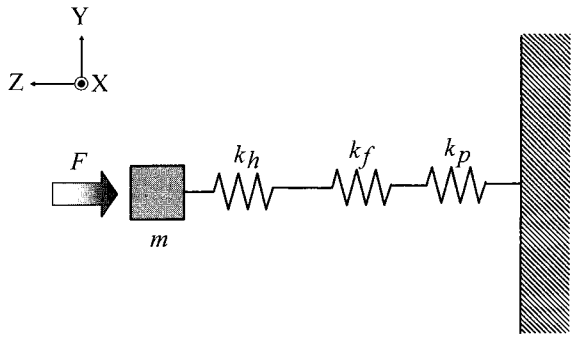

Fig. 3 Stiffness analysis model

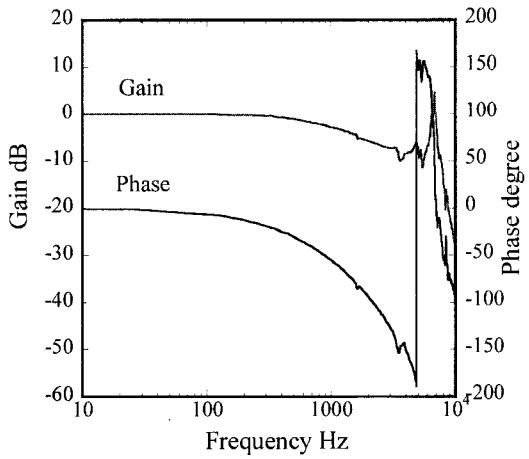

Fig. 4 Measured dynamic response of the FTC unit

where
k_h: stiffness of the head, 7319.4 N/μm;
k_f: stiffness of the force sensor, 1634.3 N/μm; and
k_p: stiffness of the PZT actuator, 117.5 N/μm.

The calculated stiffness K_Z of the FTC unit with the force sensor is 108 N/μm. Without the force sensor, k_f in Eq. (1) is infinite, resulting in a value of 115 N/μm. Thus, including the force sensor in the FTC unit does not significantly reduce its stiffness.

The dynamic response of the FTC unit is determined by both mechanical and electronic factors. The mechanical factors consist of the stiffness and mass of the FTC unit, both of which determine the resonant frequency of the FTC unit in the Z direction according to the following expression:

$$f_Z = \frac{1}{2\pi}\sqrt{\frac{K_Z}{m}} \quad (2)$$

where m is the effective mass of the moving elements and is approximately 0.113 kg. Using this value, the resonant frequence f_Z is 4920 Hz.

Experiments were carried out to confirm the dynamic response of the FTC unit by using a FFT analyzer with a bandwidth of 40 kHz. The PZT actuator was excited by a swept sine wave with an amplitude of 500 nm, a value at which the influence of electronic factors can be ignored. The outcome is shown in Figure 4. The FTC unit had a resonant frequency of approximately 4850 Hz, in good agreement with the calculated value. The measured cutoff frequency (-3 dB) was approximately 1080 Hz.

The electronic factors include the capacitance of the PZT actuator, the applied signal, and the capacity of the PZT amplifier. The maximum frequency as a result of the electronic factors is expressed by:[12]

$$f_{\max} = \frac{I_{\max}}{\pi C V_{p-p}} \quad (3)$$

where

I_{max}: maximum current of the amplifier;

C: capacitance of the PZT actuator; and

$V_{p\text{-}p}$: peak to peak voltage of the sine wave.

The capacitance of a PZT actuator is proportional its stroke. In the FTC unit, the stroke is chosen to be 50 μm under a peak-to-peak voltage of 150 V. The capacitance of the PZT is 15 μF. If the maximum current of the amplifier is 0.9 A, the calculated maximum frequency is 127 Hz when the PZT oscillates with a full-stroke amplitude. Thus, the frequency response of the FTC unit is much more dependent on electronic factors. This will be taken into consideration in the experiments used to determine the machining parameters, described in the next section.

Figure 5 shows the results of calibrating the force sensor over a range of 1.5 N. The mean sensitivity of the force sensor was 517 mV/N.

3. Fabrication of the micro-lens array

3.1 Contact detection for the tool and workpiece surface

Figure 6 shows a block diagram of the contact detection system. A lock-in amplifier was used to measure the contact force with a high degree of sensitivity.[13,14] A sinusoidal signal with a certain frequency was applied to the PZT actuator through the PZT amplifier so that the tool could be vibrated by the PZT actuator with a small amplitude when the tool was approaching the workpiece surface. The same signal from the function generator was input to the lock-in amplifier as the reference signal for the lock-in detection of the force sensor output.

The vibration frequency was changed to investigate the stability of the force sensor detected by the lock-in amplifier when the tool does not come into contact with the workpiece surface. The vibration amplitude was approximately 3 nm, and was predicted based on the PZT actuator parameters. In Figure 7, the output was stable at approximately 18 mN over a frequency range of 300 Hz to 500 Hz. Therefore, the vibration frequency can be chosen from this range to make contact between the tool and the workpiece surface. Figure 8 shows the force sensor output measured when the tool came into contact with the sample surface. In the experiment, the vibration frequency was set to 380 Hz. The cylindrical workpiece was made of aluminum alloy and had a diameter of 55 mm. The Z slide of the diamond turning machine moved the FTC unit towards the workpiece surface at a constant speed in steps of 10 nm, a value that corresponds to the resolution of the Z slide. Results of using two single-crystal diamond cutting tools with different nose radii are shown in Figure 8. The FTC unit could detect the contact to an accuracy of 10 nm with the 0.2-mm radius tool and 70 nm with the 8-μm radius tool. The contact area of the 0.2-mm radius tool on the sample surface was larger than that of the 8–μm radius tool, resulting in a larger contact force. The threshold value of the force variation for detecting the contact could be determined from the variation of the lock-in amplifier output. From the fabrication experiment

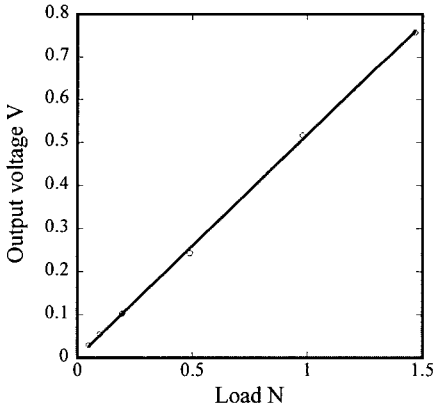

Fig. 5 Force sensor calibration

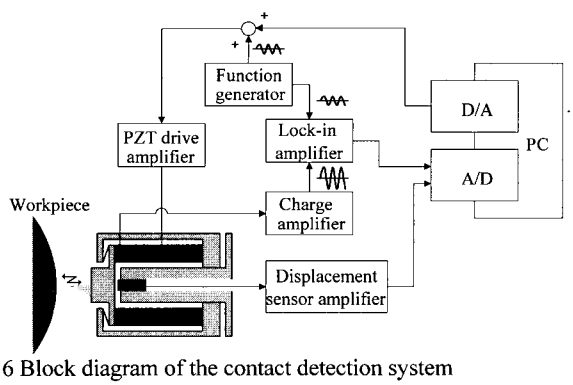

Fig. 6 Block diagram of the contact detection system

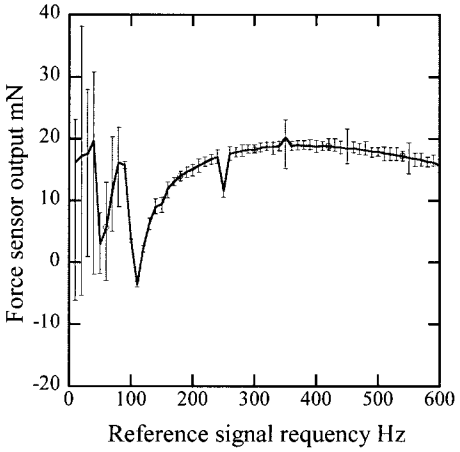

Fig. 7 Measured stability of the force sensor output detected by the lock-in amplifier

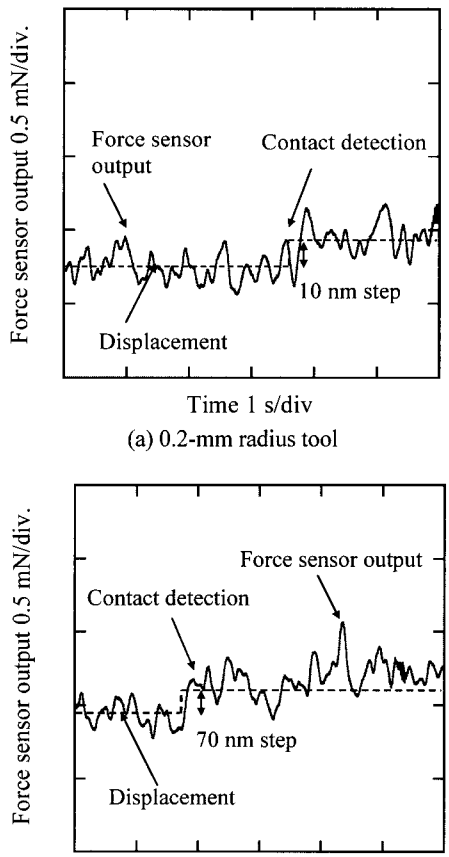

Fig. 8 Results from contact between the tool and workpiece surface

described in Section 3.3, the threshold value of the force variation was 0.2 mN. This value did not change with the workpiece material.

However, the corresponding contact displacement changed for different materials. For example, the contact displacement of aluminum was larger than nickel-phosphorus for the same threshold value of force variation because aluminium is softer.

3.2 Optimization of tool motion for the micro-lens array

Figure 9 shows a schematic diagram of the system that generated the tool motion. The FTC unit was first kept stationary at a position along the X direction so as to generate micro-lenses on a line along the circumference of the cylindrical workpiece by rotating the workpiece spindle. The FTC unit then was moved along the X direction by a micro-lens array pitch of P_A so as to generate the next line of micro-lenses along the circumference. This procedure was repeated to generate the micro-lens array on the workpiece surface over a large area.

Figure 10 shows the profile of the micro-lens surface along the axial direction (generated by the tool shape) and along the circumference (generated by the tool motion) of the workpiece. Assume that the lens length is equal to the lens pitch P_C along the circumference direction. For a fixed position x_i (i = 1, 2, ..., M) of the tool along the X direction, the cutting position along the circumference direction, which is determined by the rotary encoder of the spindle, can be expressed as:

$$\theta(j)=\frac{2\pi}{S}j \qquad j=0,1,2,\ldots,N \tag{4}$$

where S is the pulse number of the rotary encoder. If the surface profile of the micro-lens is assumed to be a parabola, the cutting motion data for the tool at position j, which corresponds to the depth of cut generated by the PZT actuator, can be calculated as follows:

$$\begin{aligned} f(j) &= a\left\{\left(r\theta(j)-nP_C\right)-\frac{P_C}{2}\right\}^2 \\ &= a\left\{\left(\frac{2\pi r}{S}j-nP_C\right)-\frac{P_C}{2}\right\}^2 \end{aligned} \tag{5}$$

where
a: constant of the parabolic profile;
P_C: pitch of lens;
n: lens number; and
r: radius of workpiece

The calculated cutting motion data are stored by the computer. When the cutting begins, the output of the rotary encoder is used as the trigger signal to transfer the cutting motion data to the FTC unit at each step.

Understanding the dynamic response of the FTC unit is important to ensure the accuracy of the micro-lens profile along the circumference direction. Figure 11 shows the displacement of the FTC unit when a parabolic signal is applied to generate a micro-lens array with a depth of 20 μm and a pitch of 190 μm. The actual amplitude was approximately 13 μm, which is 7 μm lower than the commanded amplitude. The shape generated by the FTC unit was also distorted. Thus, improvements were made to the tool path to reduce errors caused by the limited frequency response of the FTC unit, as illustrated in Figure 12. To avoid the sharp change at the intersection between two lenses, the lens array on a line along the circumference direction was generated over two rotations. The even-numbered lenses (*i.e.*, 2k, where k = 0, 1, ..., N/2) were machined in the first rotation, while the odd-numbered lenses (*i.e.*, 2k+1 where k = 0, 1,..., N/2–1) were machined in the second rotation. The data between two lenses were connected by a smooth line. Figure 13

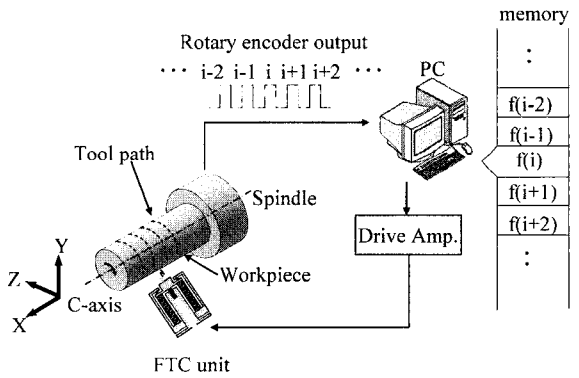

Fig. 9 System to generate the cutting motion for micro-lens array

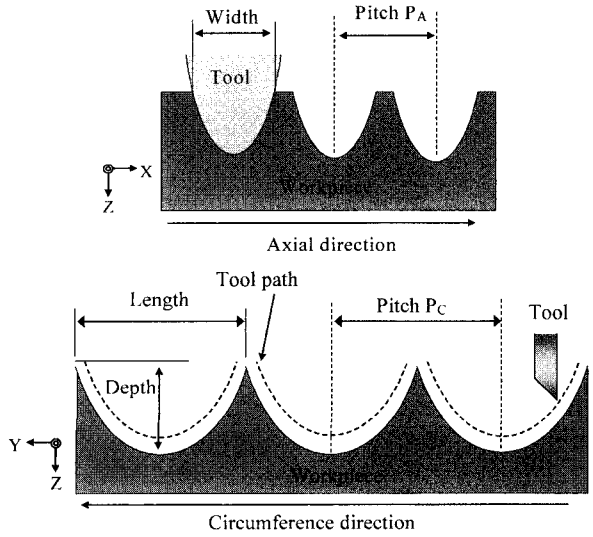

Fig. 10 Cutting motions for micro-lens arrays

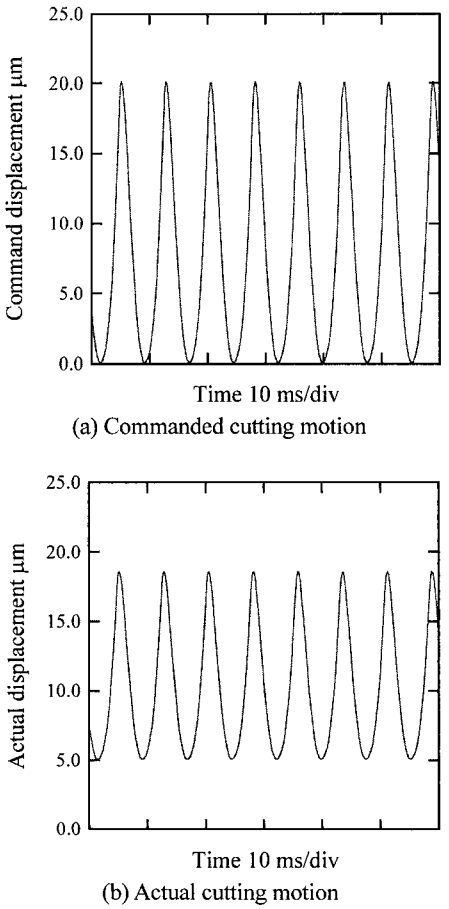

Fig. 11 Commanded and actual cutting motions along the circumference

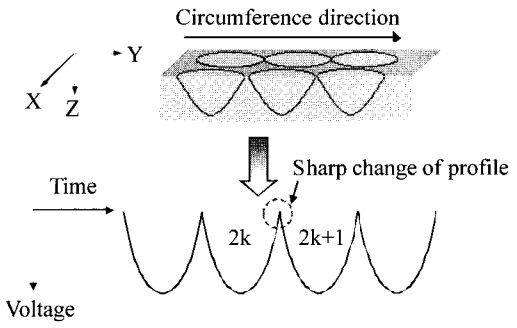

(a) Conventional command signal

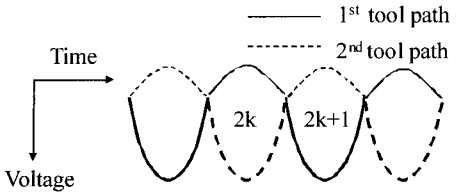

(b) Improved command signal

Fig. 12 Improving the command signal to the FTC unit

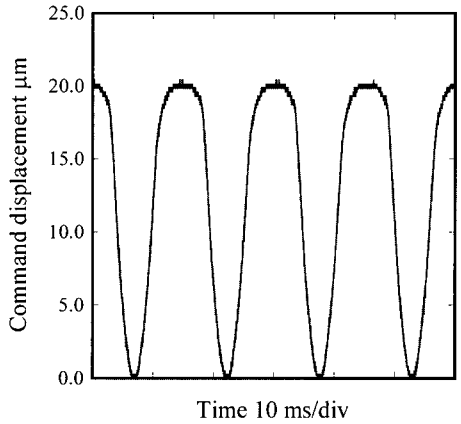

(a) Commanded cutting motion

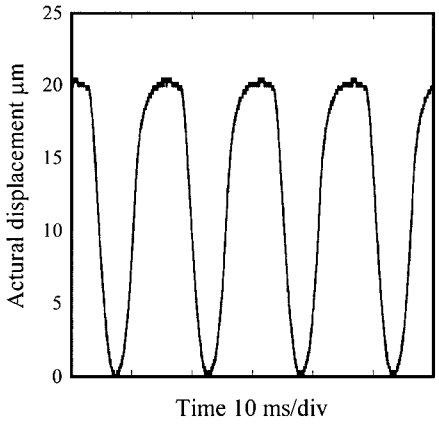

(b) Actual cutting motion

Fig. 13 Commanded and actual cutting motions of the improved tool path

shows the improved command displacement. The measured amplitude was 20.1 μm from peak to valley. The error was much smaller than that in Figure 11. The fabrication of the micro-lens array was also carried out in the open loop mode of the FTC unit to obtain a better dynamic response. However, the hysteresis characteristics of the PZT actuator generated errors in the profile of the micro-lens array in this mode. To reduce the profile error, a feed-forward compensation of the PZT displacement was employed.[15] Figure 14 shows the cutting data before the compensation was employed. They had a tracking error component of 1.2 μm. The PZT was actuated

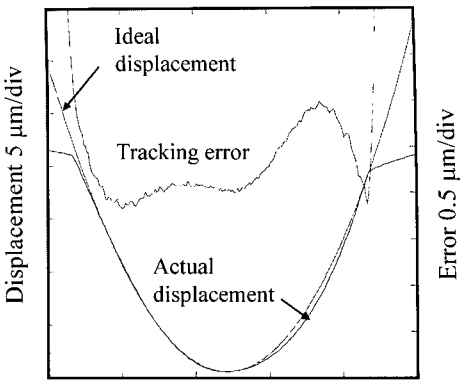

Fig. 14 Tracking error of the cutting data before compensation

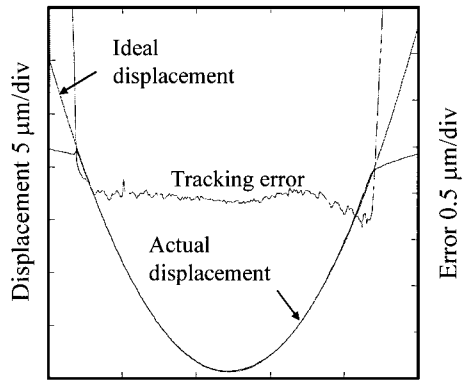

Fig. 15 Tracking error of the cutting data after compensation

with the cutting data according to the ideal profile of the micro-lens array. The displacement sensor installed in the hollow of the PZT measured the real displacement of the PZT during the actuation. The tracking error of the PZT was calculated by comparing the ideal and measured profiles from the displacement sensor. The cutting data were then corrected based on the calculated results. Figure 15 shows the cutting data after the feed-forward compensation was employed. The tracking error component was reduced from 1.2 μm to 0.3 μm.

3.3 Fabrication of the micro-lens array

In this section, experiments carried out to fabricate the micro-lens array are described. Figure 16 shows a photograph of the experimental setup. A nickel-phosphorus plating roller with an outer diameter of 55 mm was mounted on the spindle. The spindle had a rotary encoder with a pulse number of 180,000 per revolution. The X slide had a stroke of 150 mm and a resolution of 10 nm. The rotation speed of the spindle was set at 5 rpm.

Figure 17 shows a microscope image of the diamond micro-cutting tool before cutting. The nose radius of the tool was 50 μm. The rake angle was 0° and the clearance angle was 30°. First, a diamond cutting tool with a nose radius of 2 mm was mounted on the FTC unit to pre-cut the workpiece to remove its out-of-roundness component. The tool was then replaced by a micro-tool with a radius of 50 μm. After the tool came into contact with the workpiece surface, three separated lines of the micro-lens array were fabricated along the circumference of the workpiece. The improved tool path shown in Figure 13 was employed. The commanded depth was set to 20.0 μm. Figure 18 shows an image of a section of the micro-lens array. Figure 19 shows the sectional profile of the micro-lens. The lens depth was fabricated with an accuracy of 0.15 μm. The error in the depth of cut was caused mainly by the detection resolution of the initial machining position. The profile error of the micro-lens along the Z direction was related to the resolution of the initial machining position.

A large-area micro-lens array was also successfully fabricated on

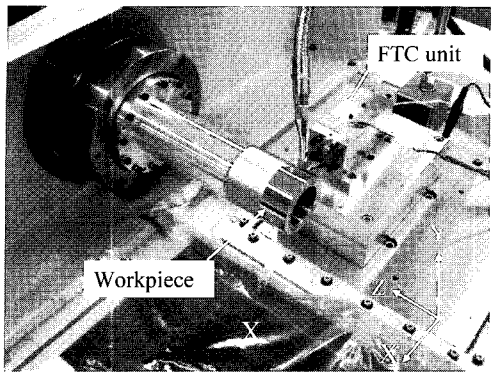

Fig. 16 Experimental setup for fabricating a large-area micro-lens array

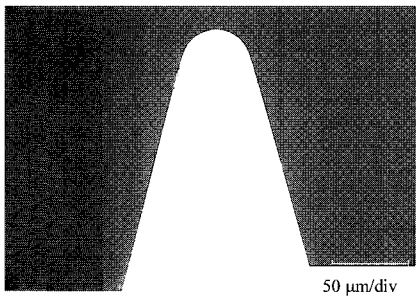

Fig. 17 Microscope image of the diamond cutting tool (R50 μm)

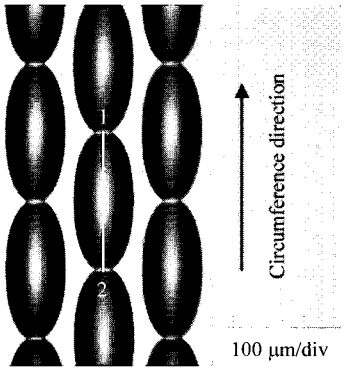

Fig. 18 Microscope image of a section of the fabricated micro-lens array

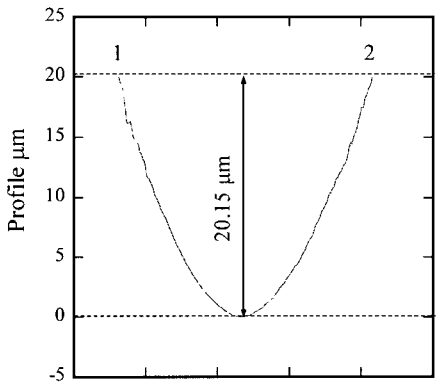

Fig. 19 Sectional profile of the micro-lens

the workpiece. Figure 20 shows a photograph of the workpiece together with an SEM image of a section of the micro-lens array that was machined on the workpiece. The lens was designed as a parabola in the circumferential direction, with a length of 190 μm, a depth of 20 μm, and a width of 80 μm. The pitches P_A and P_C were set to 50 μm and 190 μm, respectively. The fabricated area was ϕ 55 mm × 40 mm. The total time for fabrication was 27 hours. A longer fabrication time is required to produce a micro-lens array over a larger area.

4. Conclusions

A force sensor-integrated FTC unit was developed to detect the initial position of machining. The FTC unit had a full stroke of 48 μm. A feed-forward compensation technique was employed to compensate for the hysteresis characteristics of the PZT actuator.

The force sensor could detect the initial position of machining with a resolution of less than 70 nm when used with a micro-cutting tool with a nose radius of 8 μm. Using the FTC unit, a micro-lens array surface was successfully fabricated on a roller surface over an area of ϕ 55 mm × 40 mm.

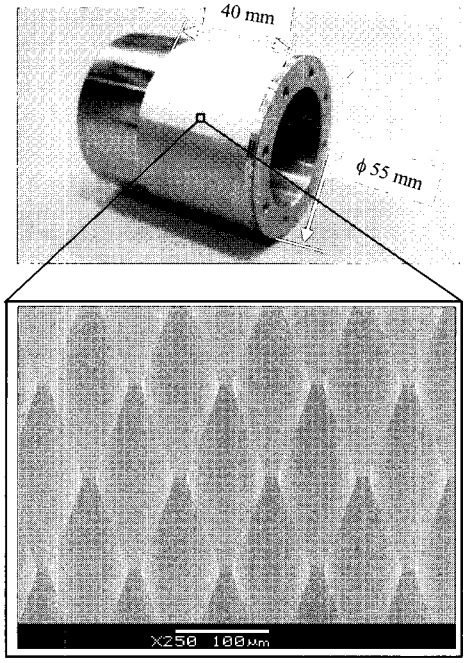

Fig. 20 Large-area micro-lens array fabricated on the workpiece

REFERENCES

1. He, M., Yuan, X. C. and Ngo, N. Q., "Single-step Fabrication of a Microlens Array in Sol-gel Material by Direct Laser Writing and its Application in Optical Coupling," Journal of Pure Optics, Vol. 6, No. 1, pp. 94-97, 2004.

2. Sim, J. H., Lee, E. D. and Kweon, H. J., "Effect of the Laser Beam Size on the Cure Properties of a Photopolymer in Stereolithography," International Journal of Precision Engineering and Manufacturing, Vol. 8, No. 4, pp. 50-55, 2007

3. Yang, R., Soper, S. A. and Wang, W. J., "Microfabrication of Pre-aligned Fiber Bundle Couplers Using Ultraviolet Lithography of SU-8," Sensors and Actuators A-Physical, Vol. 127, No. 1, pp. 123-130, 2006.

4. Dubey, A. K. and Yadava, V., "Simultaneous Optimization of Multiple Quality Characteristics in Laser Beam Cutting Using Taguchi Method," International Journal of Precision Engineering and Manufacturing, Vol. 8, No. 4, pp. 10-15, 2007.

5. Huang, Y. P., Shien, H. P. D. and Wu, S. T., "Applications of Multidirectional Asymmetrical Micro-lens Aarray Light-Control Films on Reflective Liquid Cristal Displays for Image Quality

Enhancement," Applied Optics, Vol. 43, No. 18, pp. 3656-3663, 2004.

6. Kim, D. S., Chang, I. C. and Kim, S. W., "Microscopic Topographical Analysis of Tool Vibration Effects on Diamond Turned Optical Surfaces," Precision Engineering, Vol. 26, No. 2, pp. 168-174, 2002.

7. Sharma, V. S, Dhiman, S., Sehgal, R. and Sharma, K., "Assessment and Optimization of Cutting Parameters while Turning AISI 52100 Steel," International Journal of Precision Engineering and Manufacturing, Vol. 9, No. 2, pp. 54-62, 2008.

8. http://www.precitech.com

9. Gao, W., Araki, T., Kiyono, S., Okazaki, Y. and Yamanaka, M., "Precision Nano-fabrication and Evaluation of a Large Area Sinusoidal Grid Surface for a Surface Encoder," Precision Engineering, Vol. 27, No. 3, pp. 289-298, 2003.

10. Woronko, A., Huang, J. and Altintas, Y., "Piezoelectric Tool Actuator for Precision Machining on Conventional CNC Turning Centers," Precision Engineering, Vol. 27, pp. 335-345, 2003.

11. Tano, M., Gao, W., Kimura, A., Sanuki, T., Noh, Y. J. and Kiyono, S., "Integration of a Force Sensor into a Fast-Tool-Control Unit for Fabrication of Large Area Microlens Array," Journal of the Chinese Society of Mechanical Engineers, Vol. 27, No. 5, pp. 555-560, 2006.

12. Holman, A. E., Scholte, P. M. L. O, Heerens, W. Chr. and Tuinstra, F., "Analysis of Piezo Actuator in Translation Construction," Review of Scientific Instruments, Vol. 66, No. 5, pp. 3208-3215, 1995.

13. Gao, W., Hocken, R., Patten, J. and Lucca, D., "Construction and Testing of a Nano-machining Instrument," Precision Engineering, Vol. 24, No. 4, pp. 320-328, 2000.

14. Gao, W., Hocken, R., Patten, J. and Lovingood, J., "Force Measurement in a Nanomachining Instruments," Review of Scientific Instruments, Vol. 71, No. 11, pp. 4325-4329, 2000.

15. Kim, H. S. and Kim, E. J., "Feed-forward Control of Fast Tool Servo for Real-time Correction of Spindle Error in Diamond Turning of Flat Surface," International Journal of Machine Tools & Manufacture, Vol. 43, Issue 12, pp. 1177-1183, 2003.